JCI insight

RESEARCH ARTICLE

MEG3 is increased in idiopathic pulmonary fibrosis and regulates epithelial cell differentiation

Jason J. Gokey,[1] John Snowball,[1] Anusha Sridharan,[1] Joseph P. Speth,[1] Katharine E. Black,[2] Lida P. Hariri,[3] Anne-Karina T. Perl,[1] Yan Xu,[1] and Jeffrey A. Whitsett[1]

[1]Division of Neonatology, Perinatal and Pulmonary Biology, Cincinnati Children's Hospital Medical Center, Cincinnati, Ohio, USA. [2]Pulmonary and Critical Care Medicine and [3]Department of Pathology, Massachusetts General Hospital, Boston, Massachusetts, USA.

Idiopathic pulmonary fibrosis (IPF) is a chronic interstitial lung disease causing fibrotic remodeling of the peripheral lung, leading to respiratory failure. Peripheral pulmonary epithelial cells lose normal alveolar epithelial gene expression patterns and variably express genes associated with diverse conducting airway epithelial cells, including basal cells. Single-cell RNA sequencing of pulmonary epithelial cells isolated from IPF lung tissue demonstrated altered expression of LncRNAs, including increased *MEG3*. *MEG3* RNA was highly expressed in subsets of the atypical IPF epithelial cells and correlated with conducting airway epithelial gene expression patterns. Expression of *MEG3* in human pulmonary epithelial cell lines increased basal cell–associated RNAs, including *TP63*, *KRT14*, *STAT3*, and *YAP1*, and enhanced cell migration, consistent with a role for *MEG3* in regulating basal cell identity. *MEG3* reduced expression of *TP73*, *SOX2*, and Notch-associated RNAs *HES1* and *HEY1*, in primary human bronchial epithelial cells, demonstrating a role for *MEG3* in the inhibition of genes influencing basal cell differentiation into club, ciliated, or goblet cells. *MEG3* induced basal cell genes and suppressed genes associated with terminal differentiation of airway cells, supporting a role for *MEG3* in regulation of basal progenitor cell functions, which may contribute to tissue remodeling in IPF.

Introduction

Idiopathic pulmonary fibrosis (IPF) is an interstitial lung disease causing progressive remodeling and fibrosis of the peripheral lung, leading to respiratory failure (1). Normal alveoli are lined by alveolar type 1 (AT1) cells and alveolar type 2 (AT2) cells that mediate gas exchange and secrete pulmonary surfactant into the alveolar spaces. In IPF, normal AT1 and AT2 cells are replaced by fibrotic regions, including "honeycombed" cysts, frequently lined by atypical AT2-like cells and epithelial cells of mixed cell lineages that are more characteristic of upper airway basal, goblet or ciliated cells (2, 3). Epithelial gene expression patterns in IPF are consistent with the loss of proximal-distal patterning (3). While the underlying causes of IPF remain unclear (4), transcriptomic analysis of both sorted and single epithelial cells from IPF lung tissue identified activation of a number of cellular processes involved in cell migration, proliferation, and extracellular matrix remodeling. Single-cell RNA analyses revealed gene signatures in IPF epithelial cells with characteristics of goblet, basal, and "indeterminate" cells coexpressing both alveolar and conducting airway epithelial cell–associated genes (5). Pathways regulating differentiation, cell migration, epithelial-mesenchymal transition (EMT), and proliferation, including YAP, TGF-β, mTOR/Pi3K/AKT, and WNT/planar polarity signaling were activated in IPF epithelial cells (6–11). Several of these signaling networks are regulated by long noncoding RNAs (LncRNAs), particularly in cancer (12–15).

LncRNAs are highly abundant in the human genome and are associated with regulation of cell differentiation and proliferation (16–18). LncRNAs mediate a variety of mechanisms, including gene transcription, translation, and chromatin remodeling. LncRNAs act in *cis* or *trans* to regulate gene and protein expression (19, 20). LncRNAs also interact directly with regulatory sequences, influence chromatin structure, bridge the transition from enhancers to promoters, and facilitate formation of RNA-protein complexes. Multiple LncRNAs are associated with the pathogenesis of human disease, including cancer, wherein they modulate

Authorship note: JJG and JS are co–first authors.

Conflict of interest: The authors have declared that no conflict of interest exists.

Submitted: May 29, 2018
Accepted: July 19, 2018
Published: September 6, 2018

Reference information:
JCI Insight. 2018;3(17):e122490. https://doi.org/10.1172/jci.insight.122490.

key transcription factors, such as TP53 (17–19, 21). The roles of LncRNAs in other chronic lung diseases, including IPF, are largely unknown. Therefore, we aimed to determine if LncRNAs could be playing a role in the modulation of the abnormal respiratory epithelial cells identified in our prior transcriptional analysis.

Results

Differential expression of LncRNAs in IPF epithelial cells. RNA-sequencing (RNA-seq) data from epithelial cells isolated from normal and IPF lung tissue (GEO GSE86618) were reanalyzed using a custom screen to identify LncRNAs differentially expressed in normal AT2 cells compared with the 3 distinct IPF epithelial cell types previously identified by single-cell transcriptomic studies, specifically basal-like, indeterminate, and goblet cells (5). LncRNAs (n = 21), which were differentially expressed in IPF epithelial cell types, are shown in Figure 1A. *MEG3* was the most increased LncRNA in IPF epithelial cells (Figure 1B). *MEG3* RNA varied within the IPF cell subtypes, and the highest levels of *MEG3* RNA were observed in IPF basal-like and indeterminate cells (Supplemental Figure 1; supplemental material available online with this article; https://doi.org/10.1172/jci.insight.122490DS1). All known *MEG3* RNA splicing variants were identified in IPF cells, which expressed *MEG3* at high levels (transcripts per million [TPM] >100; n = 6) (Figure 1C).

MEG3 RNA is highly expressed in IPF basal-like cells. Proximity ligation in situ hybridization (PLISH) (22, 23) was used on IPF and normal lung tissue to visualize *MEG3* RNA (Figure 2). *MEG3* RNA was detected at low levels throughout normal lung tissue and was increased in epithelial cells in IPF lungs. Immunofluorescence colocalization demonstrated increased *MEG3* RNA in IPF epithelial cells expressing basal cell markers TP63 and KRT5 (Figure 2, A and B) and in abnormal IPF AT2-like cells, which costained for ABCA3 (Figure 2A). *MEG3* was negatively correlated with NKX2.1 and was most highly expressed in airway cells expressing low levels of NKX2.1 (Figure 2C). *MEG3* was detected at low levels in $CD68^+$ immune cells and nonepithelial cells throughout the IPF lung and were not readily detected in normal lung or compared to negative control staining (Figure 2D). Analysis of RNA from $CD326^+$ epithelial cells isolated form IPF and healthy donors lungs demonstrated increased *MEG3* RNA in IPF epithelial cells (Figure 2E). Coexpression of *MEG3* RNA in $KRT5^+$ and $TP63^+$ IPF basal cells was consistent with single-cell RNA-seq, which identified expression of *MEG3* in basal and indeterminate epithelial cells.

MEG3 RNA is correlated with airway basal cell markers. Genome-wide correlation was performed to identify genes that positively or negatively correlated with *MEG3* RNA in IPF in an unbiased fashion. Spearman correlation analysis of *MEG3* with RNA profiles from IPF and donor EPCAM-sorted single cells demonstrated that normal AT2 epithelial cell markers (*STFPC*, *SFTPB*, *SFTPA1*, *SFTPD*, and *NAPSA*) and normal AT1 markers (*HOPX*) were negatively correlated with *MEG3* RNA. In contrast, *MEG3* RNA was positively correlated with basal cell–associated transcripts, *TP63*, *ITGB4*, *KRT17*, and *KRT5* (Figure 3A and Supplemental Table 1). Spearman correlation of bulk RNA sequences from CD326/HTII-280 FACS-sorted normal and IPF epithelial cells (GEO GSE94555) demonstrated that *MEG3* positively correlated with basal cell markers *TP63*, *KRT5*, *KRT17*, *KRT14*, and *ITGB4*. *MEG3* RNA was also associated with the Hippo/Yap downstream target, *AXL*. Normal AT2 cell markers *ABCA3*, *SFTPC*, and *SFTPB* were negatively correlated with *MEG3* expression (Figure 3B).

MEG3 regulates genes associated with basal cells in vitro. To test the role of *MEG3* in pulmonary epithelial cells, two *MEG3* cDNA expression constructs, one encoding the highly conserved regions present in 15 of the 16 *MEG3* splice variants and the other containing part of the conserved 5′ region and the large final exon found only in transcript 16 (T16), were transfected into HBEC3KTs, BEAS2B, and H441 human lung epithelial cell lines. *MEG3* RNA was highly expressed in cells transfected with either of the two *MEG3* cDNA expression constructs (Figure 3, C–E). Consistent with its proposed role in inducing EMT, *MEG3* increased *SNAI2* RNA in BEAS2B, HBEC3KT, and H441 cells and inhibited *CDH1* in BEAS2B and HBEC3KT cells (Figure 3C and Supplemental Figure 2). We prioritized the study of genes with predicted *MEG3*-binding sites and genes regulating epithelial cell differentiation. *MEG3* expression induced *AXL*, *KRT14*, and *TP63* in the 3 cell lines tested. Expression of *MEG3* inhibited *FOXA2* and *TP73* and increased *STAT3* and *YAP1* RNA in certain cell lines. Genes influencing differentiation of basal cells into ciliated cells (*FOXJ1*) or goblet/club cells (*MUC5AC*, *SCGB1A1*, and *SPDEF*) were not altered by *MEG3* expression in HBEC3KT cells (Supplemental Figure 2). Consistent with increased EMT-related RNAs following *MEG3* expression, cell migration was increased in HBEC3KT and BEAS2B cells, as assessed by scratch assays (Figure 4); however, *MEG3* did not alter cell proliferation of these immortalized cell lines (Supplemental Figure 3). Taken together, these data demonstrate that the LncRNA *MEG3* regulates a number of genes (*TP63*, *STAT3*, *KRT14*, *YAP1*, and *AXL*) associated with basal cell identity and increased epithelial cell migration.

A

Gene Id	Aliases	Indeterminate	Basal Like	Club/Goblet
MEG3	GTL2, LINC00023,	50.15	54.41	13.34
LINC01133	ENSG00000224259	24.30	51.64	36.29
AC006159.3	LINC01510, ENST00000458082	12.70	13.93	27.29
CTD-3252C9.4	LOC284454, AC020916.1	6.42	9.03	4.10
LINC00958	CTC-497E21.4	4.57	7.75	4.60
LINC00665	ENSG00000232677	4.99	4.97	3.48
C17orf91	MIR22HG	3.89	4.05	2.98
LINC00511	LCAL5, Onco-LncRNA-12	6.21	3.39	3.40
RP11-725D20.1	lnc-IGFBP7-7, ENST00000504537	5.01	2.71	3.31
RP11-469M7.1	lnc-BZW1-1, ENST00000568571.1	2.51	2.65	2.25
RP11-499E18.1	lnc-SLC39A8-1, ENSG00000248161	6.45	2.38	2.51
RP1-257A7.5	lnc-GFOD1-2, ENSG00000272379.1	-2.37	-2.85	-3.26
RP11-553L6.5	lnc-ZBTB20-1, ENSG00000259976	-31.48	-3.72	-54.86
AC007405.4	LINC01124, ENSG00000234350	-2.23	-5.13	-5.75
CTD-2008P7.9	lnc-IFT20-4, ENSG00000267259	-2.14	-7.19	-2.58
RP11-283C24.1	lnc-CDRT15L2-1, ENSG00000264215	-5.52	-7.25	-4.17
RP11-359M6.1	lnc-SYT1-3, ENSG00000257474	-7.19	-9.20	-6.17
CTD-2139B15.2	lnc-BASP1-1, ENSG00000248223	-4.69	-9.42	-2.69
RP11-108M9.4	lnc-MFAP2-1, ENSG00000238142	-18.33	-11.23	-3.24
RP11-462G2.1	FAM135A, ENSG00000237643	-19.69	-38.40	-10.14
RP4-782L23.1	lnc-HOOK1-1, ENSG00000231816	-6.11	Lost	-27.03
RP11-789C1.1	LINC01612, TCONS_00008319	Lost	Lost	Lost

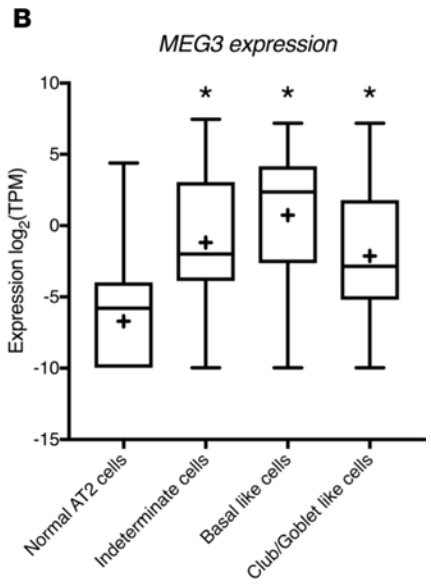

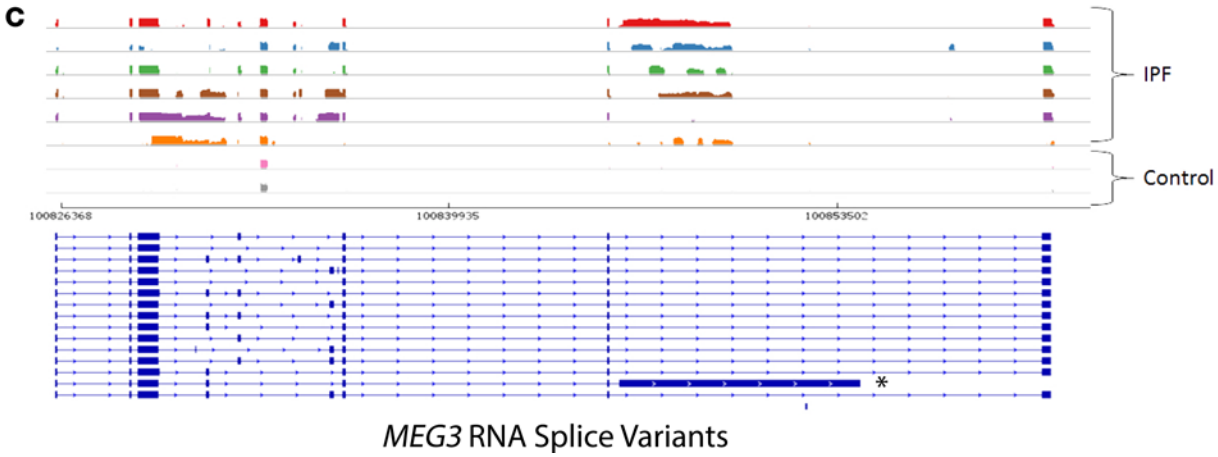

Figure 1. Altered LncRNA expression in IPF epithelial cells. (**A**) Differentially expressed LncRNAs (n = 21) were identified in single-cell RNA sequences from normal donor and IPF epithelial cells by a custom LncRNA screen (GEO GSE86618). The heatmap indicates fold changes of RNA expression in each IPF cell type. Significance was determined by ANOVA followed by Holm-Bonferroni post hoc test. $P < 0.05$. (**B**) *MEG3* RNA was most increased in indeterminate and basal-like IPF epithelial cells. Significance was determined by ANOVA followed by Holm-Bonferroni post hoc test. Box-and-whisker plots represent the first and third quartile (box), median (line), mean (+), and minimum and maximum of the data (whiskers); $^*P < 0.01$. TPM values are represented on a $\log_2$ scale. (**C**) Sashimi plots were generated by Integrative Genomics Viewer software to map reads of all known *MEG3* exons in IPF cells expressing *MEG3* RNA > 100 TPM and in 2 random control cells. All *MEG3* RNA splicing exon variants were identified in IPF epithelial cells.

MEG3-binding sites are present in the promoter regions of genes regulating airway epithelial cell differentiation. To identify potential *MEG3* targets in lung epithelial cells from IPF patients, *MEG3* DNA-binding sites previously identified by chromatin oligo affinity precipitation (ChOP) sequencing (14) were compared with single-cell RNA-seq analyses of IPF and normal AT2 epithelial cells (5). *MEG3* DNA-binding peaks were identified in 2,124 gene promoter regions (Supplemental Table 2A). Of these, 73 genes were differentially expressed in IPF (Supplemental Table 2B). *MEG3* ChOP peaks were identified in the promoter regions of *AXL*, *FOXA2*, and basal cell genes (*ITGB4*, *KRT15* and *KRT19*), all of which were significantly altered in abnormal IPF epithelial cells (Figure 5A). *MEG3*-binding sites were identified between the TA/ΔNTP63 splice sites, located after the third exon of *TAP63* and before the *ΔNTP63* alternative start site (Figure 5A). To test the potential role of *MEG3* in regulation of TP63 splicing, TP63 isoforms were detected by immunoblotting in HBEC3KT cells, which actively express multiple TP63 isoforms (24). Expression of *MEG3* inhibited ΔNTP63 protein variants, while TATP63 splice variants were not altered (Figure 5, C and D). Immunoblotting revealed that expression of TP63 isoforms was not altered in Beas2b or H441 cells. ΔNTP63 and TATP63 were assessed at the transcriptional level in pulmonary cell lines, primary human bronchial

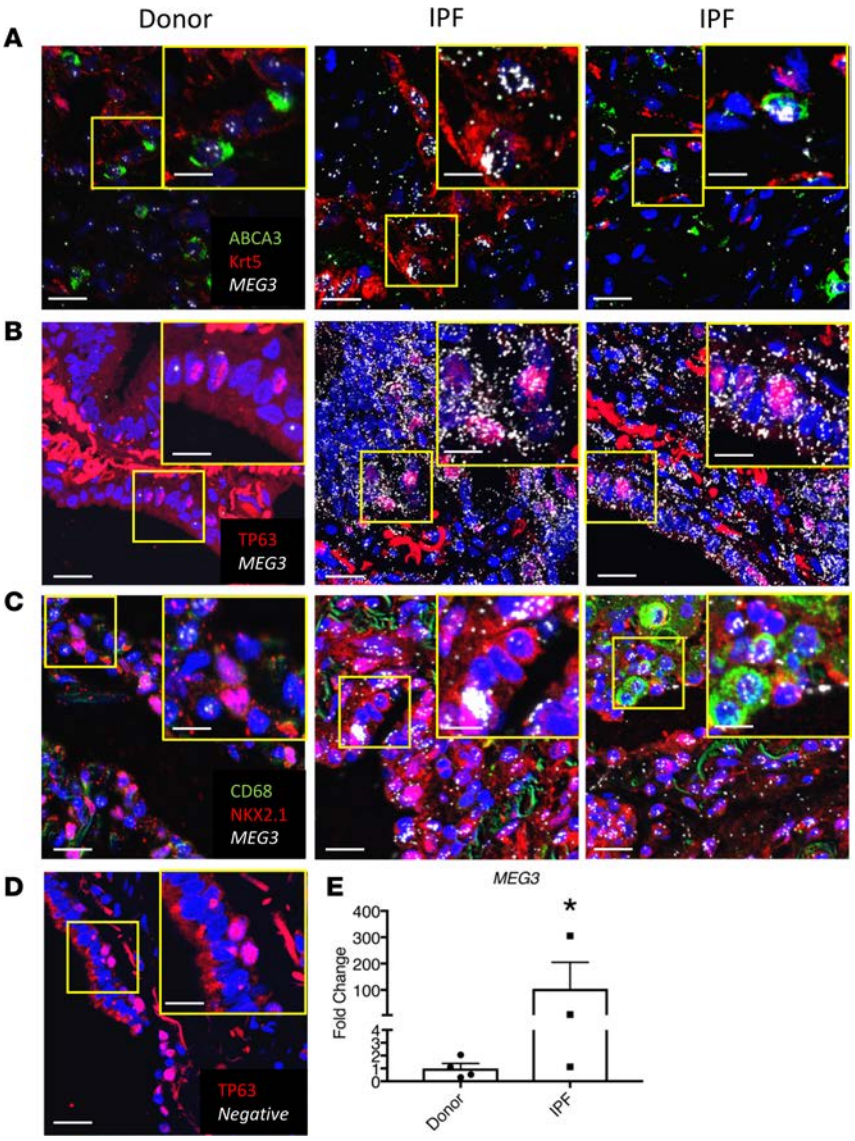

Figure 2. Colocalization of *MEG3* RNA with basal epithelial cell markers. *MEG3* RNA was identified by proximity ligated in situ hybridization (PLISH) and costained with immunofluorescence markers in normal and IPF lung tissue. (**A**) *MEG3* (white) is shown with the AT2 cell marker ABCA3 (green) and the basal cell marker KRT5 (red). *MEG3* RNA was colocalized in the atypical AT2 cells and KRT5$^+$ basal cells in IPF. (**B**) *MEG3* (white) colocalized with the basal cell marker, TP63 (red). (**C**) Low levels of *MEG3* RNA (white) were detected in epithelial cells expressing NKX2.1 (red) and in CD68$^+$ macrophages (green). (**D**) A bacteria *Bacillus subtilis* gene *mgsA* target probe was used as a negative control for PLISH (white) and TP63 (red). Images are representative of n = 6 donors and n = 8 IPF patient samples. (**E**) Quantification of *MEG3* RNA from CD326$^+$-sorted epithelial cells isolated from IPF (n = 3) and healthy donor (n = 4). A 1-tailed Mann-Whitney t test was used to determine significance of increased *MEG3* RNA expression. *$P < 0.05$. Images were obtained at ×60 magnification.

epithelial cells (HBECs) cells, and CD326$^+$ epithelial cells isolated from IPF and healthy donors. ΔNTP63 was slightly reduced in HBEC3KTs, and TATP63 RNA was increased in HBEC3KT and Beas2b cell lines (Supplemental Figure 4A). TP63 splice isoforms were not altered in HBEC cells, consistent with total TP63 being unaltered in these cells (Supplemental Figure 4B). ΔNTP63 and TATP63 were increased in CD326$^+$ epithelial cells isolated from donors and IPF lungs, although levels of TATP63 were increased at a higher level (Supplemental Figure 4C). Promoter regions of genes associated with basal cell differentiation, i.e., *SOX2*, *STAT3*, *FOXN4*, *FOXA1*, *TP73*, and *HEY1*, and genes involved in EMT (*SNAI2*, *SNAI1*, and *CDH1*) contained predicted *MEG3*-binding sites (Figure 5B and Supplemental Table 2B). Taken together these data support a potential role for *MEG3* in regulating basal cell differentiation and promoting EMT in IPF.

MEG3 suppresses genes associated with basal cell differentiation in primary airway epithelial cells. Primary HBECs were transfected with *MEG3* cDNA constructs. RNAs with *MEG3*-binding sites in their gene promoters and RNAs associated with basal cell differentiation were assessed. Genes associated with basal cell differentiation; *TP73*, a regulator of ciliated cell differentiation; and the Notch target *HEY1* were inhibited by *MEG3* (Figure 6). In donor DD011L, TP73 was expressed at low levels at baseline and was not significantly altered by *MEG3*. Other Notch targets, *NRARP* and *HEY1*, were inhibited by *MEG3* T16. In certain donors, *MEG3* induced *SNAI2*, a gene associated with EMT, and regulated *SOX2* depending on *MEG3* expression levels (Supplemental Figure 5). Genes associated with basal cells that were induced in HBEC3KTs, BEAS2B, and H441, i.e., *TP63* and *KRT14*, were not altered by

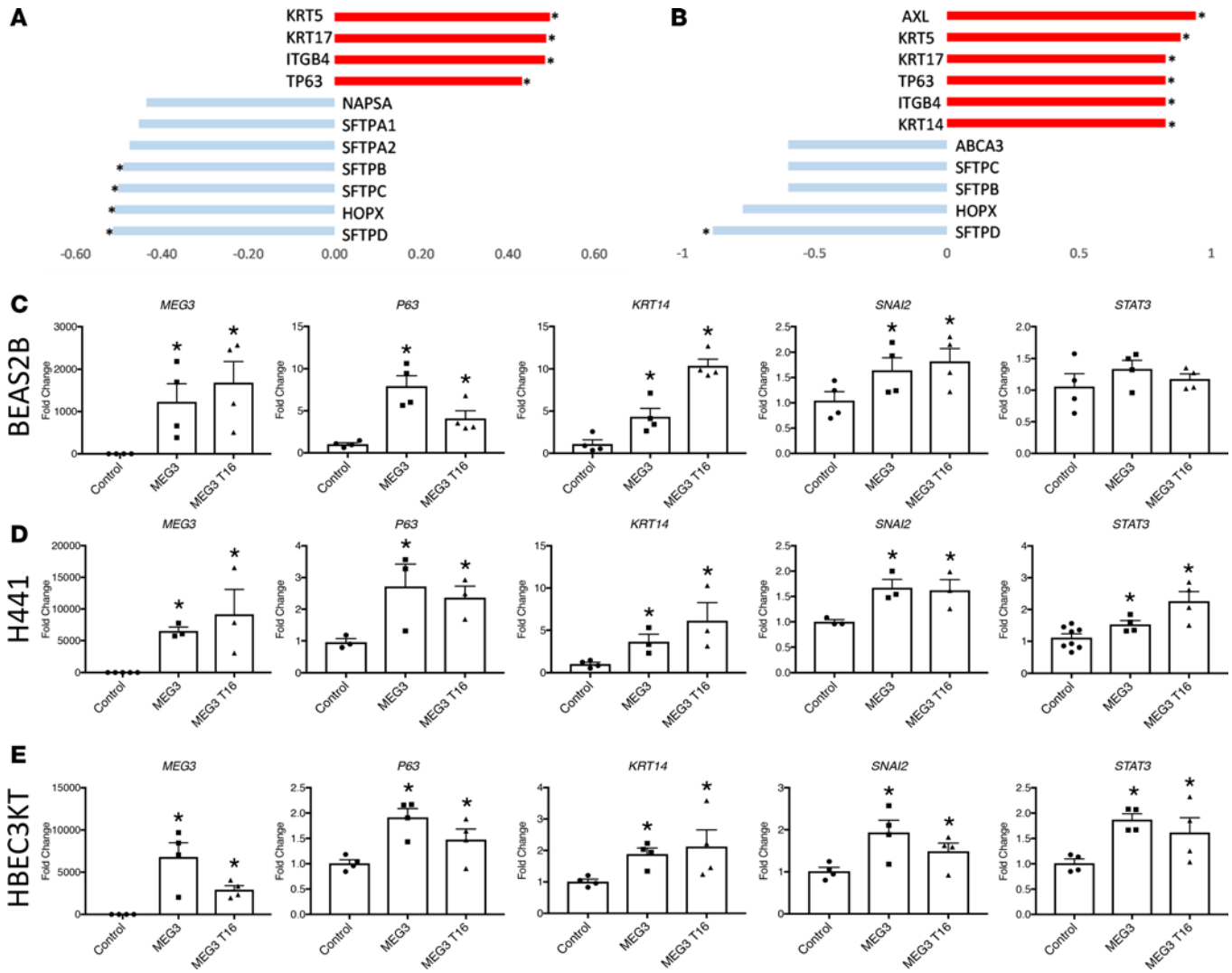

Figure 3. *MEG3* RNA is correlated with RNAs associated with basal cells. (**A**) Correlation of *MEG3* RNA (Spearman correlation) with all genes identified in CD326⁺-sorted single-cell RNA sequencing from normal donor and IPF epithelial cells (GEO GSE86618) was performed using R software's correlation function. A selection of the top 50 positive and negative Spearman correlation coefficients was visualized in graphical format. *MEG3* was correlated with basal cell markers (*KRT5*, *KRT17*, *ITGB4*, and *TP63*) and was negatively correlated with normal alveoli markers (*NAPSA*, *SFTPA1*, *SFTPA2*, *SFTPB*, *SFTPC*, *SFTPD*, and *HOPX*). (**B**) Spearman correlation was performed on RNA from FACS-sorted AT2 cells from IPF and control lungs (GEO GSE94555). *MEG3* correlated with basal cell markers, i.e., *KRT5* and *TP63*, and negatively correlated with markers of differentiated alveolar epithelial cells, *SFTPC* and *HOPX*. (**C**–**E**) *MEG3* cDNA was expressed in (**C**) BEAS2B, (**D**) H441, and (**E**) HBEC3KT cells. *MEG3* induced basal cell–associated genes (*TP63*, *KRT14*, and *STAT3*) and EMT-associated gene *SNAI2*. $^*P < 0.05$, as determined by ANOVA; n = 3–4 wells transfected and n = 4 transfections for each cell line.

MEG3 expression in primary HBEC cultures (Supplemental Figure 5). In contrast to cell lines, *AXL* was inhibited in primary HBEC cells collected from a subset of donors expressing *MEG3*. These results indicate a potential role for *MEG3* in the regulation of basal cell differentiation.

Predicted transcriptional regulatory network active in IPF epithelial cells. We previously demonstrated increased expression of genes associated with active canonical TGF-β, HIPPO/YAP, PI3K/AKT, and WNT signaling in IPF epithelial cells (5, 11). We further predicted cross talk among these activated signaling pathways and formed a transcriptional regulatory network (TRN) predicted to influence the differentiation of IPF epithelial cells. Transcription factors, including TGF-β1, TP53/63, CTNNB1, and NFKB, and ETS family members (SPDEF, ETV5, EHF) were predicted to serve as important regulatory hubs in the IPF epithelial network (5). In the present work, the effects of *MEG3* on the IPF network were assessed by modeling the interactions between *MEG3* and the IPF TRN. As shown, *MEG3* was predicted to interact with and influence expression of a number of important regulators of the IPF network (Figure 7). Some of these interactions were previously reported in other biological systems (black lines, Figure 7). For example, previous in vitro studies

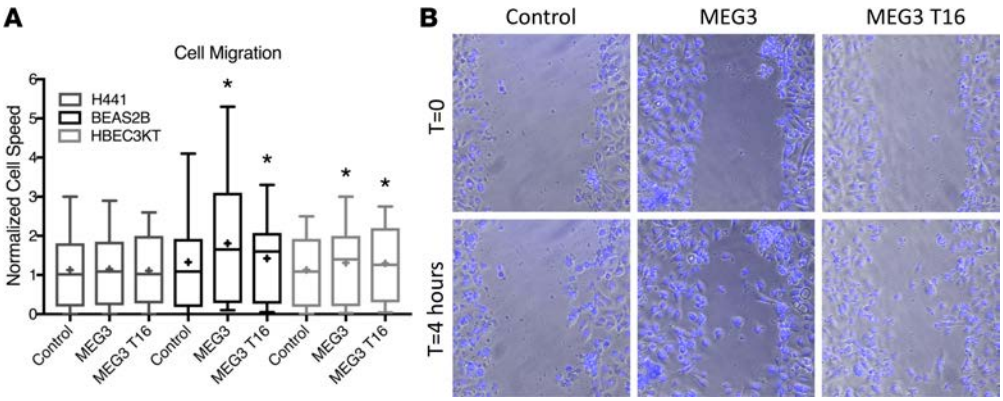

Figure 4. *MEG3* expression increases cell migration. *MEG3* cDNA was expressed in HBEC3KT, H441, and BEAS2B cells. (**A**) Cell migration was assessed by scratch assay in HBEC3KT, H441, and BEAS2B cell lines transfected with MEG3 cDNA. *MEG3* increased cell migration in HBEC3KT and BEAS2B cells. Cell migration is presented as cell speed normalized to empty vector–transfected control for each cell line. (**B**) Representative images of HBEC3KT cells transfected with *MEG3* at 0 and 4 hours following scratch assay. Differences were determined by an ANOVA. $*P < 0.05$, $n = 3–4$ wells transfected and $n = 3$ transfections for each cell line. Average cell speed was calculated by Imaris cell tracking software. Over 10,000 cells were tracked for each transfection. Graphs represent an average of 3 separate experiments. Box-and-whisker plots represent the first and third quartile (Box), median (line), and minimum and maximum (whiskers) of each data set. Images were obtained at ×10 magnification.

demonstrated that *MEG3* interacts directly with *TP53*, *EZH2*, and *TGFβ* (12, 14, 15). Our current data predicts interactions between *MEG3* and genes in the IPF TRN (green lines, Figure 7), wherein *MEG3* positively regulates *TP63*, *YAP1*, *SNAI2*, and *STAT3* and negatively regulates *FOXA2* and *TP73* (Figure 7). SPDEF, a key transcription factor required for goblet cell differentiation in the airways, inhibits *MEG3* expression in pulmonary adenocarcinoma cells (25). Together, the network analysis suggests that *MEG3* plays an important regulatory role in the TRN in epithelial cells and likely influences abnormal epithelial cell differentiation in IPF.

Discussion

Herein, we identified 21 human LncRNAs that were significantly altered in IPF epithelial cells compared with those isolated from normal donor lung. Of these LncRNAs, *MEG3* was highly induced in $KRT5^+$ and $TP63^+$ indeterminate and basal cells in IPF and was rarely detected in normal lung epithelial cells. *MEG3* RNA was positively correlated with basal cell gene expression and was negatively correlated with alveolar epithelial markers, supporting the concept that *MEG3* is coexpressed with and influences basal cell gene expression. In vitro expression of *MEG3* in various lung epithelial cell lines enhanced *TP63*, *AXL*, and *KRT14* RNAs, while expression of genes associated with terminal differentiation of the basal progenitor cell, i.e., *FOXJ1*, *SCGB1A1*, or *SPDEF*, was not altered. *MEG3* induced genes involved in the specification and renewal of progenitor basal cells, including *YAP1* and *STAT3* (26–29). Expression of *MEG3* cDNA did not further induce genes associated with basal cells in primary HBEC cells; however, genes associated with basal cell differentiation into ciliated, club, or goblet cells (*TP73*, *SOX2*, *HEY1*, *HES1*, and *NRARP*) were significantly ($P < 0.05$) inhibited by *MEG3*. Taken together, these findings support the concept that the LncRNA *MEG3* regulates expression of pulmonary airway epithelial cell genes associated with the basal-like state, typical of the peripheral lung in IPF (Figure 8).

Since the loss of lung architecture in IPF is characterized by heterogeneous and extensive fibrosis, attention has generally focused on mechanisms of fibroblast proliferation, survival, and differentiation. However, there is increasing genetic and experimental evidence supporting a critical role for cell survival and differentiation of the respiratory epithelial cells in the pathogenesis of IPF (1, 30–32). In the present work, we found that *MEG3* RNA was increased more than 50-fold in atypical basal and indeterminate cells in IPF and was frequently associated with coexpression of genes normally restricted to atypical respiratory epithelial cell types, supporting the concept that these cells have lost normal cell "lineage fidelity" (33). During normal lung development and repair, alveolar and conducting epithelial cells maintain highly strict lineage relationships that distinguish conducting, compared with alveolar, regions of the lung. Severe and recurrent alveolar injury, such as influenza infection or repeated exposure to lung

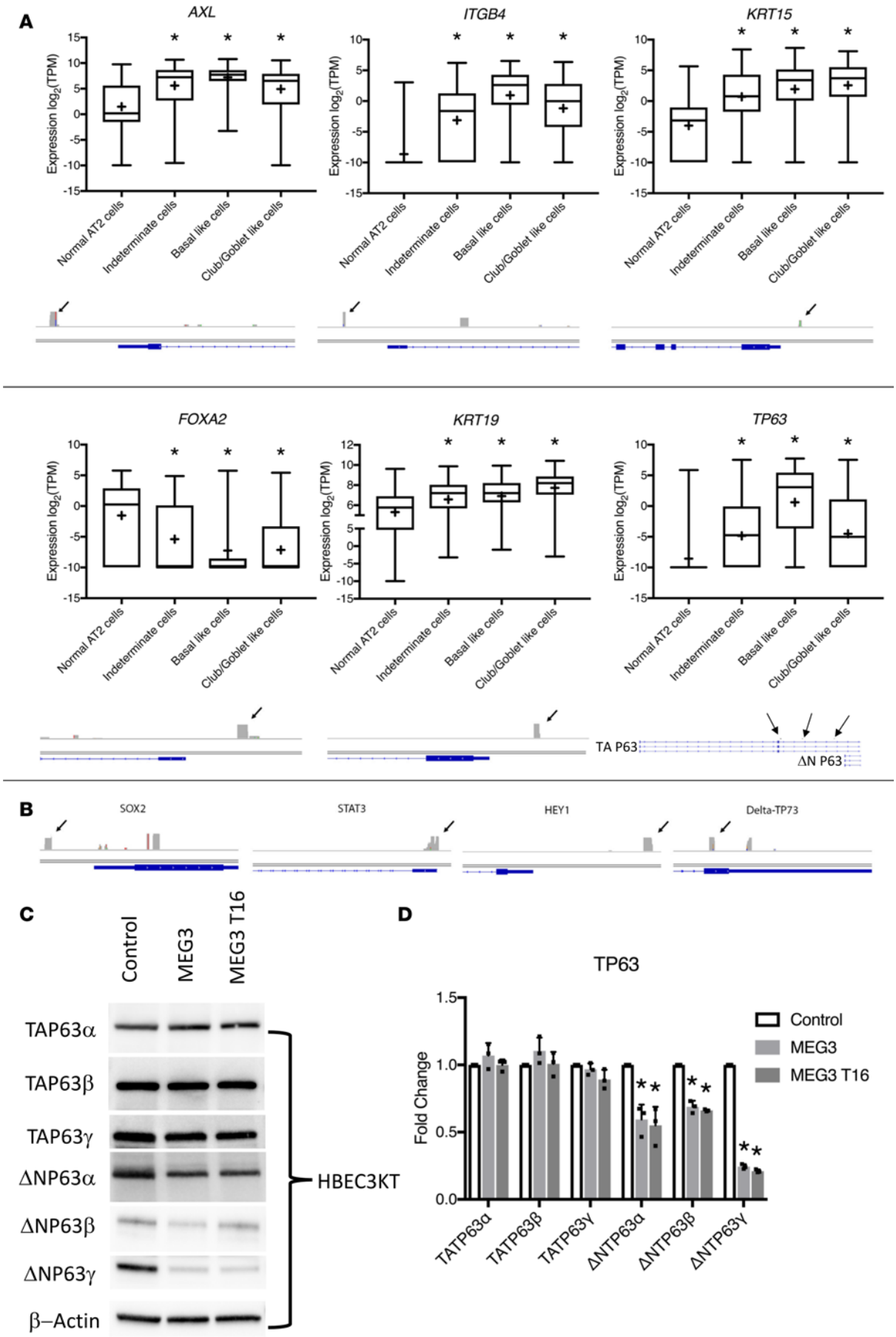
A
AXL
ITGB4
KRT15
FOXA2
KRT19
TP63
Expression log2(TPM)
Normal AT2 cells
Indeterminate cells
Basal like cells
Club/Goblet like cells
TA P63
ΔN P63
B
SOX2
STAT3
HEY1
Delta-TP73
C
Control
MEG3
MEG3 T16
TAP63α
TAP63β
TAP63γ
ΔNP63α
ΔNP63β
ΔNP63γ
β–Actin
HBEC3KT
D
TP63
Fold Change
Control
MEG3
MEG3 T16
TATP63α
TATP63β
TATP63γ
ΔNTP63α
ΔNTP63β
ΔNTP63γ

Figure 5. MEG3-binding sites in the promoters of genes associated with basal cell differentiation. ChOP-sequencing data of *MEG3*-binding sites in BT-549 cells (14) were analyzed using Homer's *Annotate Peak* and visualized using integrated genomics viewer to reveal *MEG3*-binding sites in gene promoters and compared with differentially expressed genes identified by analyzing single-cell RNA sequencing of IPF and control lungs, as described in the Methods. *MEG3*-binding sites within promoters (arrows) were identified in genes (blue) associated with basal cells, including *AXL*, *ITGB4*, *KRT15*, *KRT19*, and *FOXA2*, which are altered in IPF. *MEG3*-binding sites were detected in the promoters of *SOX2*, *STAT3*, and *HEY1* and in the TA/ΔN splicing region of *TP63* and *TP73*, as shown as gray peaks with arrows in the gene maps. (**A**) Expression of basal cell–associated genes in IPF epithelial cell types from single-cell sequencing (5) and location of *MEG3*-binding sites curated from ChOP data (14). Box-and-whisker plots represent the first and third quartile (box), median (line), mean (+), and minimum and maximum of the data (whiskers). TPM expression values are represented on a $\log_2$ scale. (**B**) Location of *MEG3*-binding sites in the promoters of *STAT3*, *SOX2*, and *HEY1* and before the ΔN *TP63* and *TP73* start sites. Peaks were visualized using Integrative Genomics Viewer software. (**C**) Western blots of *MEG3*-transfected HBEC3KT cells were used to assess TP63 splice variants. (**D**) *MEG3* transfection inhibited levels of all ΔNTP63 isoforms and did not alter TAP63 isoforms in HBEC3KT cells. Differences in RNA expressions were determined by ANOVA followed by Holm-Bonferroni post hoc test. $^*P < 0.01$.

toxicants, activates alternative repair processes, causing proliferation and migration of atypical basal cells into alveolar regions that fail to restore normal alveolar epithelial cell structure and function (34–37). Expression of *MEG3* in HBEK3KT and BEAS2B cells induced cell migration and basal cell signature genes *TP63* and *KRT14* as well as Hippo pathway genes *AXL* and *YAP1*. *TP63* is a central transcriptional regulator of the airway basal cells, regulating basal cell migration and regeneration of the airway epithelia after injury (35–37). Along with *TP63*, a number of transcriptional signaling pathways regulate the function and differentiation of basal cells, including YAP and Notch. Increased expression of YAP caused hyperproliferation of basal cells and blocked their differentiation, whereas loss of YAP caused terminal differentiation and loss of the progenitor cell populations (26–28). Herein, we demonstrate a *MEG3*-binding site in the promoter region of the YAP target gene *AXL* and induction of *YAP1* and *AXL* following *MEG3* expression in pulmonary epithelial cell lines in vitro. *AXL* is a receptor tyrosine kinase directly regulated by the YAP pathway that may play a role in basal cell population maintenance (38). Increased *YAP1* and *AXL* RNA following MEG3 expression in vitro indicates a potential role for *MEG3* in enhancing YAP signaling and therefore basal cell identity. In addition to enhanced YAP signaling in IPF, *SOX2* expression and Notch signaling regulate basal cell differentiation (27, 39, 40). Deletion of *SOX2* in airway epithelial cells prevented *SCGB1A1* and *FOXJ1* expression, consistent with the requirement of *SOX2* in differentiation of both club and ciliated cells (39). *SOX2* activity in conducting airways is dependent on upstream Notch signaling (41). Notch controls the fate of basal cells, as low Notch activity causes differentiation of basal cells into ciliated cells through activation of TP73 and FOXJ1 (42, 43). Increased Notch activity causes differentiation of basal progenitor cells into goblet or often secretory cells (40, 44, 45). In the present study, *MEG3* suppressed Notch targets *HES1*, *NRARP*, and *HEY1* and reduced *TP73* and *SOX2*, supporting a role for *MEG3* in a gene network regulating basal cell differentiation. The presence of ChOP-binding sites in the promoters of basal cell–associated genes, e.g., *SOX2*, *KRT15*, *STAT3*, *FOXA2*, and *HEY1* supports a potential direct role for *MEG3* in regulation of basal cell differentiation. Although the factors regulating *MEG3* are unknown at present, expression of SPDEF in A549 cells induced goblet cell–associated genes and repressed *MEG3* RNA (25). Several microRNAs (miRs) regulate *MEG3*, including *miR-148a* and *miR-29* in cancer; the latter is regulated by the Hippo/YAP pathway (46–48). Hypoxic conditions and HIF1α enhanced expression of *MEG3* in human umbilical endothelial cells (49, 50). Increased YAP activity (11) and hypoxemia may contribute to the increased expression of *MEG3* in IPF epithelial cells (51, 52).

Presently, the observed strong correlation between *MEG3* and basal cell–associated genes supports the concept that *MEG3* plays a role in influencing basal cell identity, contributing to the loss of epithelial cell lineage specification in IPF. The present study demonstrated that expression of *MEG3* increased *TP63* in several pulmonary epithelial cell lines. In contrast, *MEG3* inhibited *TP73*, a critical regulator of ciliated cell fate in primary HBEC cells. Present immunoblotting data demonstrated that *MEG3* decreased all 3 ΔNTP63 splice variants in the HBEC3KT cell, a cell line that actively expresses *TP63* (24). Both TP63 and TP73 genes have multiple splice variants, with the ΔN splice forms having alternate start sites. (53–55). We identified *MEG3*-binding sites before the transcriptional start sites of both TP63 and TP73 ΔN splicing variants in *MEG3* ChOP data (14). The presence of *MEG3*-binding sites and inhibition of ΔNTP63 by *MEG3* in HBEC3KT cells supports a potential role for *MEG3* in transcript-specific regulation of *TP63*. Although the specific functions of TP63 and TP73 splice variants are unclear at the present, both TATP63 and ΔNTP63 increased basal cell migration and keratin expression in vitro (34, 37, 56, 57). ΔNTP73 may act as a dominant negative regulator of TATP73, thus inhibiting ciliated cell differentiation (58).

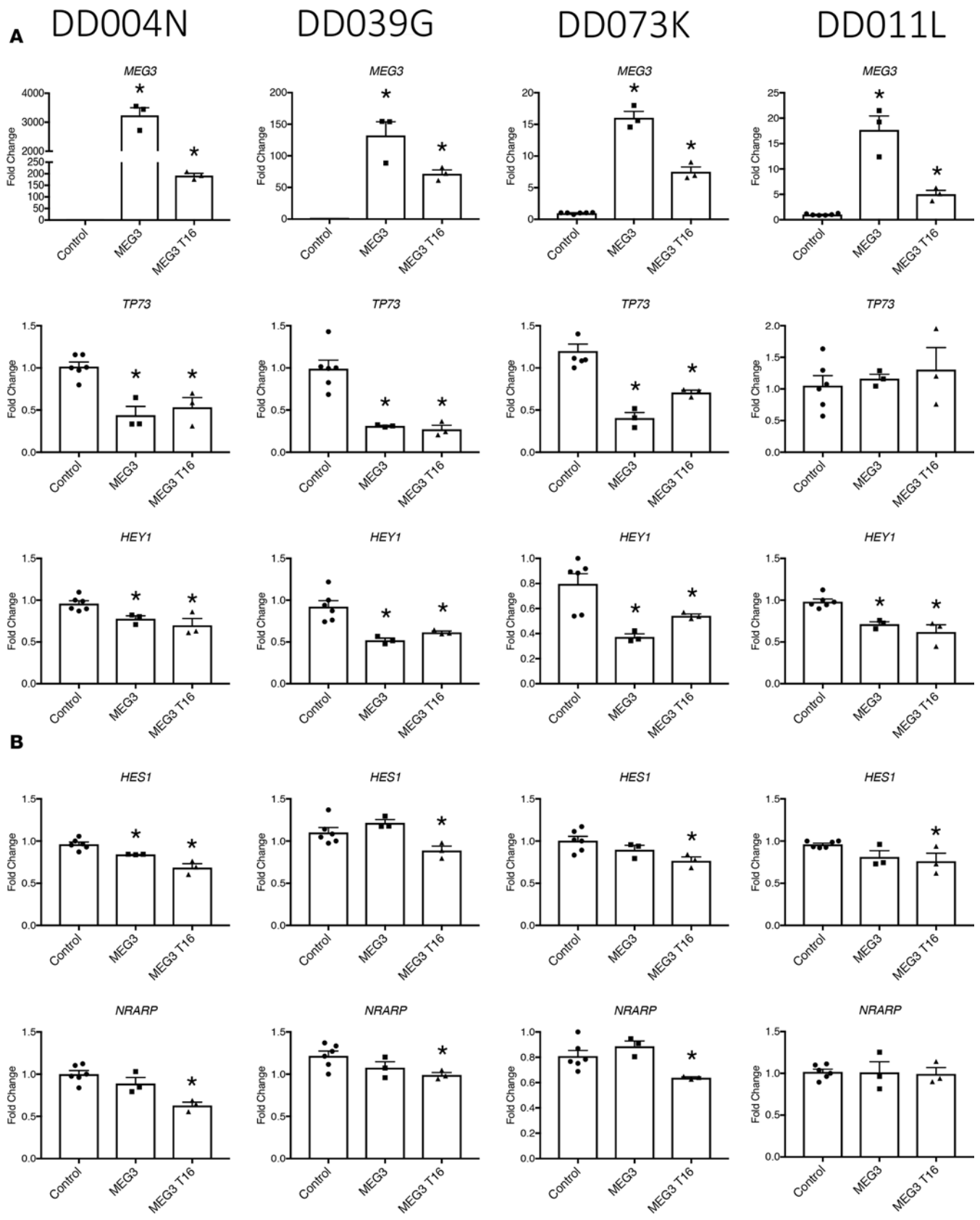

Figure 6. *MEG3* inhibits *TP73*, *HES1*, *HEY1*, and *NRARP* in primary HBEC cells. *MEG3* cDNA was transfected into primary donor human bronchial epithelial (HBEC) cells (donor identifiers, DD04N, DD039G, DD073K, and DD011L). RNA was collected 48 hours after transfection. (**A**) *TP73* and the Notch target *HEY1* were inhibited by the expression of *MEG3* cDNA. (**B**) Notch targets *HES1 and NRARP* were inhibited by *MEG3* transcript 16. Differences in RNA expression were determined by ANOVA. $^*P < 0.05$; $n = 3$ wells transfected for each expression construct and $n = 4$ donors are shown.

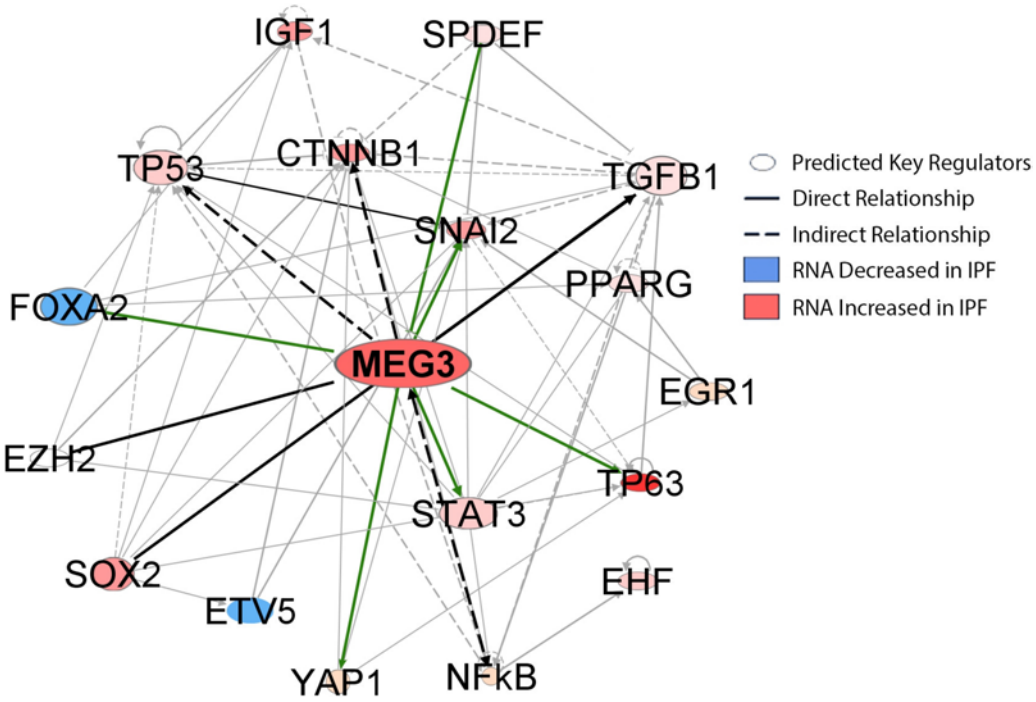

Figure 7. *MEG3* is predicted to interact within a regulatory network in IPF. *MEG3* was integrated into a previously generated IPF network of predicted key regulators active in CD326/HTII-280 FACS-sorted IPF and control epithelial cells using Ingenuity Pathway Analysis (IPA) software suite's Path Designer and Genomatix (5). Black and gray lines represent relationships determined by IPA Ingenuity knowledge base literature mining or Genomatix. Green lines indicate interactions presently reported.

In the present study, we found that *MEG3* increased cell migration and regulated EMT-associated genes, for example, increasing *YAP1*, *STAT3*, and *SNAI2* and reducing *CDH1* (59, 60). ChOP identified *MEG3*-binding sites in the promoters of *SNAI1*, *SNAI2*, and *CDH1*, indicating potential direct epigenetic regulation of EMT-associated genes by *MEG3*, supporting previous studies demonstrating that *MEG3* regulates EMT genes in lung cancer (61). In IPF lungs, a partial EMT phenotype is observed, wherein epithelial cells acquire mesenchymal features and epithelial-mesenchymal crosstalk is enhanced (62–64). EMT, the biological process in which polarized epithelial cells transition into motile fibroblast-like cells, is active during normal development, lung repair, organ fibrosis, and in the initiation of metastasis (65–67). Loss of *CDH1* and increased cell migration are fundamental events in EMT (59). Recent single-cell sequencing suggested the activation of an EMT gene network in IPF that likely contributes to the pathogenesis of the disease (5). Increased cell migration and transcriptional changes of EMT-associated genes following *MEG3* expression support a role for *MEG3* in enhancing EMT, which may contribute to the pathogenesis of IPF.

Herein, we demonstrate that *MEG3* is likely connected with a gene network regulating epithelial cell gene expression, migration, and EMT. Long noncoding RNAs like *MEG3* regulate both transcriptional and translational activity (16, 17, 20). *MEG3* forms an RNA-DNA triplex and alters chromatin methylation and gene expression by recruiting EZH2 in lung cancer (61). ChOP-sequencing analysis revealed putative *MEG3*-binding sites throughout the genome of BT-549 cells (14). The abundance of *MEG3*-binding sites identified in BT-549 cells by ChOP indicates that *MEG3* likely plays context-dependent, pleiotropic roles in regulating gene expression. Previously defined roles for *MEG3* in chromatin methylation, regulating both active H3K4me1 and inactivation H3K27me3 marks, may influence expression of genes associated with the basal cell identity in IPF (14). Previous analysis of IPF epithelial cells demonstrated activation of several signaling pathways, including YAP, TGF-β, mTOR/Pi3K/AKT, and WNT/polarity (5, 11). *MEG3* increases TGF-β signaling by increasing TGF-β target gene expression through recruitment of EZH2 (14, 61) and activates mTOR/Pi3K/AKT through inhibition of PTEN and β-catenin in cancer (13, 15). We demonstrated that *MEG3* increased *YAP1* and *AXL* mRNAs in H441 and BEAS2B pulmonary adenocarcinoma cells, consistent with our recent findings that YAP signaling is increased in IPF epithelial cells (11).

In summary, we identified 21 altered LncRNAs in IPF epithelial cells. *MEG3* was highly expressed in subsets of IPF epithelial cells. ChOP analysis identified predicted *MEG3*-binding sites in the promoters of genes associated with a network regulating basal cell differentiation. *MEG3* RNA was correlated with basal cell–associated genes (for example, *TP63*, *SOX2*, *STAT3*, and *KRT14*) and induced EMT/cell migration–related genes (i.e., *SNAI2* and *YAP1*), all of which are predicted to interact in a network activated in IPF epithelial

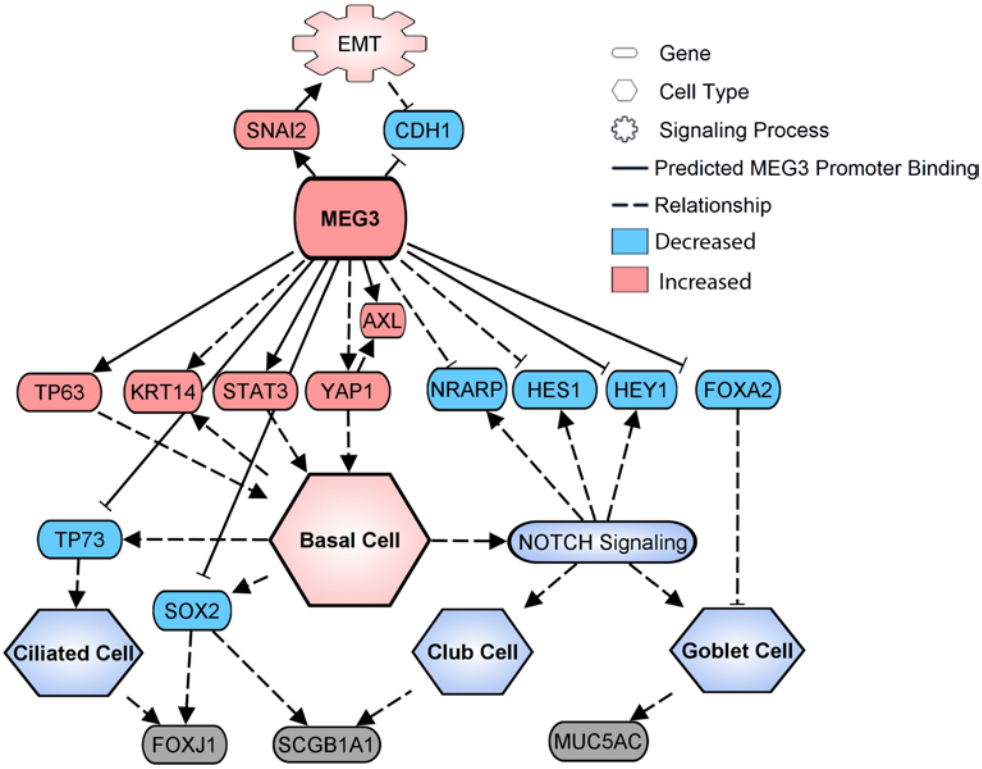

Figure 8. Proposed mechanism by which *MEG3* regulates basal cell differentiation. *MEG3* regulates genes that promote basal cell specification and renewal, while preventing basal cell differentiation. In vitro, expression of *MEG3* induces known basal cell markers (*KRT14*) and genes that promote basal cell self-renewal, *TP63*, *YAP1*, and *STAT3*, while genes associated with basal cell differentiation into ciliated (*FOXJ1*), club (*SCGB1A1*), or goblet cells (*MUC5AC*) are not changed. *SOX2*, Notch signaling, and *TP73* are known to play an active role in basal cell differentiation. In primary HBEC cells *TP73*, *SOX2*, and Notch signaling targets *HES1* and *HEY1* are inhibited by *MEG3* expression, predicting inhibition of basal cell differentiation by *MEG3*. Relationships are based on presently reported RNA changes induced by *MEG3* expression in vitro.

cells. Although varying among epithelial cell types studied, expression of *MEG3* in vitro regulated TP63 splicing and directly activated *TP63*, *STAT3*, *AXL*, and EMT-associated genes *SNA2*, *CDH1*, and *YAP1*. These findings are consistent with the activation of an atypical airway-associated gene expression pattern in the peripheral lung of patients with IPF. Taken together, the present findings support a role for *MEG3* in the regulation of a gene network modulating pulmonary epithelial cell identity and differentiation in IPF.

Methods

IPF and normal lung tissue. Deidentified IPF patient explant tissue was provided through the Massachusetts General Hospital Transplant Biorepository. Samples were selected based on clinical diagnosis of IPF according to guidelines set by the American Thoracic Society, with usual interstitial pneumonia confirmed after examining the pathology of explants, with no other underlying cause identified. Deidentified healthy nonsmoking donor samples were collected from resected lungs rejected for transplant and were provided by Scott Randell, University of North Carolina at Chapel Hill, Chapel Hill, North Carolina, USA, in accordance with the CFF Tissue Procurement and Cell Culture Core (CFF BOUCHE15R0). Primary HBECs were also acquired from Scott Randell in accordance with the NIH CFRTCC Cell Models Core (NIH P30DK065988).

Single-cell RNA-seq data generation. Single-cell RNA-seq data from human IPF and normal lung epithelial cells were analyzed using SINCERA analytic pipeline as described previously (5, 69). Both raw data sets (GEO GSE86618) and interpreted data are freely available at the LGEA web portal (https://research.cchmc.org/pbge/lunggens/mainportal.html).

LncRNA screen of single-cell data. The LncRNA screen was performed by generating a gene matrix comprised of all 540 single cells and their corresponding gene expressions. A standard Student's *t* test was performed comparing each of the 3 IPF cell clusters to the normal AT2 cell cluster. For each comparison, genes with a $P < 0.001$, a fold change >2, and an average TPM >1 were considered differentially expressed. Genes that were differentially expressed in all 3 comparisons and had fold changes in the same direction were deemed as differentially expressed in IPF abnormal cell types, resulting in 726 genes that passed our criteria for differential expression. Classification of the differentially expressed genes found the majority (625 genes) were protein coding, and 23 were classified as LncRNA based on gene annotation from Ingenuity Pathway Analysis suites (IPA). The LncRNAs identified were further assessed by ANOVA, followed by the Holm-Bonferroni post hoc test, resulting in 21 differentially expressed LncRNAs in IPF epithelial cells.

Bioinformatics analyses. IPA suite's Path Designer and Genomatix were used to create predictive models and networks. Samtools and Integrative Genomics Viewer (Broad Institute) were used to create indexed bam files and exon coverage plots from CD326$^+$ sorted single-cell sequence data. Exon coverage plots were shown on a log scale. Genomatix's MatInspector was used for promoter analysis. Correlation patterns were calculated in R using the correlation function, specifying Spearman correlation on both AT2-sorted bulk RNA and CD326$^+$ sorted single-cell RNA using cells that expressed *MEG3* TPM >1 to reduce background noise. Genes were then ranked according to their correlation values. *MEG3* promoter-binding sites were found by reanalyzing publicly available *MEG3* ChOP data (14). *MEG3*'s ChOP Bam file was converted to a Bed file using Bedtools. The resulting Bed file was analyzed using Homer's *find peaks* function followed by Homer's *annotate peaks* function (69). Peaks in annotated promoter regions were prioritized and were compared with differentially expressed genes in IPF to identify potential direct targets of *MEG3* (Supplemental Figure 2B).

Multiplex fluorescent in situ hybridization (PLISH). IPF and normal donor lung tissues were fixed in 4% paraformaldehyde/1× PBS overnight, dehydrated in graded ethanol washes, and then embedded in paraffin. Paraffin-embedded IPF and donor tissue samples were sectioned at 5 μm and were pretreated with 10 mM citrate buffer (pH 6.0) for antigen retrieval. PLISH was performed as previously reported (11, 22, 23). In short, the protocol was performed as follows: labeled hybridization probes (Supplemental Table 3) were incubated at concentrations of 100 nM each in hybridization buffer (1 M sodium trichloroacetate [NaTCA], 5 mM EDTA, 50 mM Tris [pH 7.4], 0.2 mg/ml heparin in DEPC water) for 2 hours at 37°C and 100% humidity. Sections were incubated with T4 ligase buffer (NEB, catalog M0202) and phosphorylated common bridge and connector circle oligos at 10 nM for 60 minutes. Subsequent incubations were performed with ligase buffer and T4 ligase for 2 hours under the same conditions. DNA amplification was accomplished using Phi-29 polymerase (Lucigen-30221) in polymerase buffer using the same conditions overnight. After the reaction was complete, slides were washed with label buffer (2× SCC/20% formamide in DEPC water) and incubated with 100 nM Tye705 label probe in label probe buffer for 1 hour using the same conditions. Immunofluorescent costaining and images were obtained by confocal microscopy (Nikon A1R LUN-V inverted microscope) and analyzed. Negative controls included secondary antibody alone and reactions performed with identically labeled probes for the bacteria Bacillus subtilis gene *mgsA*. Target probes were ordered with standard desalting. Fluorophore-conjugated label probes, connecting circles, and the common bridge were HPLC purified, and stored as 100 μM stocks (IDT Inc.).

Immunofluorescence imaging. Immunofluorescence confocal microscopy was performed following PLISH. Samples were blocked in 4% normal donkey serum in PBS, 0.1% Triton-X (PBST), 5 mM EDTA for 1 hour at room temperature. Slides were incubated in primary antibodies (Supplemental Table 4) diluted in blocking buffer for 24–48 hours at 4°C. Samples were washed in PBST (3 times). Secondary antibody (1:200) and DAPI (1mg/ml) were added for 2 hours at room temperature. Samples were washed in PBST (3 times for 5 minutes each) and rinsed in phosphate buffer, and cover slips were mounted with Prolong Gold (Thermo Fisher Scientific). Images were captured on an inverted Nikon A1R confocal microscope (×20 or ×60 magnification). Maximum intensity projections of *Z*-stack images were generated using NIS-Elements software (Nikon).

Cell culture and transfection. HBEC3KT (a gift from J.D. Minna, University of Texas Southwestern Medical Center, Dallas, Texas, USA) cells were grown in keratinocyte serum-free growth media, and BEAS2B (ATCC) and H441 cells were cultured in RPMI media (Thermo Fisher Scientific). Two different partial *MEG3* expression plasmids were used for transfection. The conserved *MEG3* plasmid encoding the conserved 5′ region and another encoding the 3′ region specific to T16 were used. Both constructs contained a proposed EZH2-binding site (14). Cells were transfected with 1 μg of either the conserved region of *MEG3* (pCI-*MEG3*) (Addgene, catalog 44727), pCI empty vector, *MEG3* T16 (pCMV6-XL5-*MEG3*) (OriGene, catalog SC116343), or empty pCMV6-XL vector with 4 μl/ml FuGene HD transfection reagent (Promega, catalog E2311) in cell culture media. Samples were collected 48 hours after transfection. All cell lines were transfected in 3 independent experiments. For RNA analysis, 3–4 wells were used per transfection and 2 wells were used per transfection for protein analysis. Primary HBECs, provided by Dr. Scott Randell, were cultured as previously described on collagen-coated plates (27). Passage-2 cells were transfected with 0.5 μg or 1 μg of the above *MEG3* or empty vector plasmids by electroporation using the Neon system (Thermo Fisher Scientific). Transfections were done in 24-well plates, in triplicate, and were harvested for RNA analysis 48 hours after transfection.

TaqMan qRT-PCR RNA analysis. Patient lung tissue epithelial cells were isolated using CD326$^+$ magnetic beads (Miltenyi Biotec, catalog 130-061-101). RNA from sorted cells or cell culture experiments was extracted using the RNeasy Micro kit (Qiagen) with on-column DNase I treatment, and cDNA was syn-

thesized using 500–1,000 ng RNA input using the iScript cDNA synthesis kit (Bio-Rad). TaqMan qPCR was performed using a StepOne Plus Real-Time PCR system (ABI 7500) utilizing TaqMan gene expression assays (Supplemental Table 5) (Thermo Fisher Scientific). All samples were assayed in duplicate for each target gene, target genes were normalized to 18s values of corresponding samples, and relative expression was assessed using ΔΔCT quantification method.

Western blot analysis. Cells were lysed in RIPA buffer (Thermo) containing phosphatase and protease inhibitors (Roche). Protein concentration was determined using DirectDetect (Millipore) infrared system. For Western blots, 10%–20% tris/glycine gels (Invitrogen) were used to separate proteins and 25 μg protein was loaded per sample. Protein was transferred using the iBlot system (Invitrogen) onto a PVDF membrane. Membranes were blocked using 5% BSA diluted in TBS + 0.1% Tween (TBST) for 1 hour. Primary antibodies (Supplemental Table 5) were diluted in 0.5% BSA in TBST and incubated at 4°C degrees over-night. Membranes were washed 3 times for 10 minutes in TBST at room temperature, and corresponding HRP-conjugated secondary antibody was added for 1 hour. Membranes were washed 3 times for 10 minutes in TBST. Chemiluminescence was detected using Illuminata Crescendo or Classico HRP substrates (Millipore), and the membranes were digitally imaged on a Chemidoc Touch imager (Bio-Rad). Detected bands were assessed for correct target protein molecular weight and quantified using Imagelab software (Bio-Rad) and normalized to β-actin.

Cell migration and proliferation analyses. For cell migration assays, cells were grown to 100% confluence following transfection with *MEG3* expression constructs. The confluent monolayer was scratched using a p20 pipette tip. Cells were imaged on a SpectraX wide-field microscope for 16 hours with image acquisition every 10 minutes. Cell migration speed was determined using Imaris cell-tracking software. To determine average cell speed, $n > 10{,}000$ cells were tracked for each treatment. For proliferation analysis, transfected cells were seeded on 12-well plates at a density of 20,000 cells/well. Cells were counted 48 hours later to assess proliferation.

Statistics. For qRT-PCR, proliferation, and migration assays, ANOVA followed by a Tukey post hoc test was used to determine significance between pCI empty vector and pCI *MEG3* conserved or pCMV empty vector and pCMV *MEG3* T16, as determined by $P < 0.05$. In each analysis, pCI and pCMV empty vectors were not significantly different. For statistical purposes, data from control empty vectors were pooled together. Error bars indicate mean ± SEM values. Student's *t* tests were 2-tailed.

Study approval. Deidentified IPF patient explant tissue was provided through the Massachusetts General Hospital Transplant Biorepository. The protocol was reviewed and approved by the Partners Institutional Review Board, Boston, Massachusetts, USA, and informed consent was obtained from each subject in accordance with the Partners Institutional Review Board (2013P002332). Deidentified healthy nonsmoking donor lungs were acquired from Scott Randell, University of North Carolina at Chapel Hill, in accordance with the CFF Tissue Procurement and Cell Culture Core (CFF BOUCHE15R0). The Cincinnati Children's Hospital Medical Center Institutional Review Board declared that donor tissue samples were Institutional Review exempt, in accordance with protocol 2013-3356.

Author contributions

JJG designed, performed, analyzed, and interpreted experiments and wrote and edited the manuscript. JS designed and performed bioinformatics analyses, interpreted experiments, and wrote and edited the manuscript. AS designed, performed, and analyzed experiments and edited the manuscript. JPS performed experiments. KEB provided IPF samples and edited the manuscript. LPH provided IPF samples, edited the manuscript, and performed pathological analysis to confirm IPF samples. AKTP designed experiments and edited the manuscript. YX designed and guided bioinformatics analyses, interpreted data, and edited manuscript. JAW designed experiments, interpreted data, and wrote the manuscript.

Acknowledgments

The authors thank Scott Randell for providing normal donor patient samples and Jenna Green and Jillian Spinney for their assistance in processing the patient samples. The authors thank the patients and families who selflessly donated the tissue samples. Funding for this project was provided by NIH grants T32 HL007752 (to JJG and JAW), U01 HL122642 (to JAW, AKTP, and YX), U01 HL122638 (to JAW, AKTP, and YX), U01 HL134745 (to JAW, AKTP, and YX), and R01 HL131661 (to Jenna Green, YX, JS, and AKTP). Additionally, Translational Fibrosis Academic and Research Committee funding was from the Cincinnati Children's Hospital Medical Center.

Address correspondence to: Jeffrey A. Whitsett or Yan Xu, 3333 Burnet Avenue, Cincinnati, Ohio, 45229, USA. Phone: 513.803.2790; Email: jeffrey.whitsett@cchmc.org (J.A. Whitsett). Phone: 513.636.8921; Email: yan.xu@cchmc.org (Y. Xu).

1. Kropski JA, Blackwell TS, Loyd JE. The genetic basis of idiopathic pulmonary fibrosis. *Eur Respir J*. 2015;45(6):1717–1727.
2. Plantier L, et al. Ectopic respiratory epithelial cell differentiation in bronchiolised distal airspaces in idiopathic pulmonary fibrosis. *Thorax*. 2011;66(8):651–657.
3. Seibold MA, et al. The idiopathic pulmonary fibrosis honeycomb cyst contains a mucocilary pseudostratified epithelium. *PLoS ONE*. 2013;8(3):e58658.
4. Wolters PJ, et al. Time for a change: is idiopathic pulmonary fibrosis still idiopathic and only fibrotic? *Lancet Respir Med*. 2018;6(2):154–160.
5. Xu Y, et al. Single-cell RNA sequencing identifies diverse roles of epithelial cells in idiopathic pulmonary fibrosis. *JCI Insight*. 2016;1(20):e90558.
6. Barkauskas CE, Noble PW. Cellular mechanisms of tissue fibrosis. 7. New insights into the cellular mechanisms of pulmonary fibrosis. *Am J Physiol, Cell Physiol*. 2014;306(11):C987–C996.
7. Grimminger F, Günther A, Vancheri C. The role of tyrosine kinases in the pathogenesis of idiopathic pulmonary fibrosis. *Eur Respir J*. 2015;45(5):1426–1433.
8. Xu X, et al. Rapamycin increases CCN2 expression of lung fibroblasts via phosphoinositide 3-kinase. *Lab Invest*. 2015;95(8):846–859.
9. Piersma B, Bank RA, Boersema M. Signaling in Fibrosis: TGF-β, WNT, and YAP/TAZ Converge. *Front Med (Lausanne)*. 2015;2:59.
10. Yan Z, Kui Z, Ping Z. Reviews and prospectives of signaling pathway analysis in idiopathic pulmonary fibrosis. *Autoimmun Rev*. 2014;13(10):1020–1025.
11. Gokey JJ, et al. Active epithelial Hippo signaling in idiopathic pulmonary fibrosis. *JCI Insight*. 2018;3(6):98738.
12. Xia Y, He Z, Liu B, Wang P, Chen Y. Downregulation of Meg3 enhances cisplatin resistance of lung cancer cells through activation of the WNT/β-catenin signaling pathway. *Mol Med Rep*. 2015;12(3):4530–4537.
13. Zheng Q, et al. Long noncoding RNA MEG3 suppresses liver cancer cells growth through inhibiting β-catenin by activating PKM2 and inactivating PTEN. *Cell Death Dis*. 2018;9(3):253.
14. Mondal T, et al. MEG3 long noncoding RNA regulates the TGF-β pathway genes through formation of RNA-DNA triplex structures. *Nat Commun*. 2015;6:7743.
15. Yang NQ, Luo XJ, Zhang J, Wang GM, Guo JM. Crosstalk between Meg3 and miR-1297 regulates growth of testicular germ cell tumor through PTEN/PI3K/AKT pathway. *Am J Transl Res*. 2016;8(2):1091–1099.
16. Huarte M. The emerging role of lncRNAs in cancer. *Nat Med*. 2015;21(11):1253–1261.
17. Wapinski O, Chang HY. Long noncoding RNAs and human disease. *Trends Cell Biol*. 2011;21(6):354–361.
18. Schmitt AM, Chang HY. Long noncoding RNAs in cancer pathways. *Cancer Cell*. 2016;29(4):452–463.
19. Rinn JL, Chang HY. Genome regulation by long noncoding RNAs. *Annu Rev Biochem*. 2012;81:145–166.
20. Bartonicek N, Maag JL, Dinger ME. Long noncoding RNAs in cancer: mechanisms of action and technological advancements. *Mol Cancer*. 2016;15(1):43.
21. Tsai MC, Spitale RC, Chang HY. Long intergenic noncoding RNAs: new links in cancer progression. *Cancer Res*. 2011;71(1):3–7.
22. Nagendran M, Riordan DP, Harbury PB, Desai TJ. Automated cell-type classification in intact tissues by single-cell molecular profiling. *Elife*. 2018;7:e30510.
23. Nabhan AN, Brownfield DG, Harbury PB, Krasnow MA, Desai TJ. Single-cell Wnt signaling niches maintain stemness of alveolar type 2 cells. *Science*. 2018;359(6380):1118–1123.
24. Ramirez RD, et al. Immortalization of human bronchial epithelial cells in the absence of viral oncoproteins. *Cancer Res*. 2004;64(24):9027–9034.
25. Guo M, et al. Gene signature driving invasive mucinous adenocarcinoma of the lung. *EMBO Mol Med*. 2017;9(4):462–481.
26. Mahoney JE, Mori M, Szymaniak AD, Varelas X, Cardoso WV. The hippo pathway effector Yap controls patterning and differentiation of airway epithelial progenitors. *Dev Cell*. 2014;30(2):137–150.
27. Lange AW, Sridharan A, Xu Y, Stripp BR, Perl AK, Whitsett JA. Hippo/Yap signaling controls epithelial progenitor cell proliferation and differentiation in the embryonic and adult lung. *J Mol Cell Biol*. 2015;7(1):35–47.
28. Zhao R, et al. Yap tunes airway epithelial size and architecture by regulating the identity, maintenance, and self-renewal of stem cells. *Dev Cell*. 2014;30(2):151–165.
29. Kida H, et al. GP130-STAT3 regulates epithelial cell migration and is required for repair of the bronchiolar epithelium. *Am J Pathol*. 2008;172(6):1542–1554.
30. Li M, et al. Epithelium-specific deletion of TGF-β receptor type II protects mice from bleomycin-induced pulmonary fibrosis. *J Clin Invest*. 2011;121(1):277–287.
31. Wang Y, et al. Genetic defects in surfactant protein A2 are associated with pulmonary fibrosis and lung cancer. *Am J Hum Genet*. 2009;84(1):52–59.
32. Madala SK, et al. Rapamycin regulates bleomycin-induced lung damage in SP-C-deficient mice. *Pulm Med*. 2011;2011:653524.
33. Ge Y, et al. Stem cell lineage infidelity drives wound repair and cancer. *Cell*. 2017;169(4):636–650.e14.
34. Zuo W, et al. p63(+)Krt5(+) distal airway stem cells are essential for lung regeneration. *Nature*. 2015;517(7536):616–620.
35. Chilosi M, et al. Abnormal re-epithelialization and lung remodeling in idiopathic pulmonary fibrosis: the role of deltaN-p63. *Lab Invest*. 2002;82(10):1335–1345.
36. Rock JR, et al. Basal cells as stem cells of the mouse trachea and human airway epithelium. *Proc Natl Acad Sci USA*. 2009;106(31):12771–12775.
37. Arason AJ, et al. deltaNp63 has a role in maintaining epithelial integrity in airway epithelium. *PLoS One*. 2014;9(2):e88683.

38. Cui ZL, et al. YES-associated protein 1 promotes adenocarcinoma growth and metastasis through activation of the receptor tyrosine kinase Axl. *Int J Immunopathol Pharmacol*. 2012;25(4):989–1001.
39. Tompkins DH, et al. Sox2 activates cell proliferation and differentiation in the respiratory epithelium. *Am J Respir Cell Mol Biol*. 2011;45(1):101–110.
40. Rock JR, Gao X, Xue Y, Randell SH, Kong YY, Hogan BL. Notch-dependent differentiation of adult airway basal stem cells. *Cell Stem Cell*. 2011;8(6):639–648.
41. Tsao PN, Vasconcelos M, Izvolsky KI, Qian J, Lu J, Cardoso WV. Notch signaling controls the balance of ciliated and secretory cell fates in developing airways. *Development*. 2009;136(13):2297–2307.
42. Jackson PK, Attardi LD. p73 and FoxJ1: programming multiciliated epithelia. *Trends Cell Biol*. 2016;26(4):239–240.
43. Nemajerova A, et al. TAp73 is a central transcriptional regulator of airway multiciliogenesis. *Genes Dev*. 2016;30(11):1300–1312.
44. Borggrefe T, Oswald F. The Notch signaling pathway: transcriptional regulation at Notch target genes. *Cell Mol Life Sci*. 2009;66(10):1631–1646.
45. Chen G, et al. SPDEF is required for mouse pulmonary goblet cell differentiation and regulates a network of genes associated with mucus production. *J Clin Invest*. 2009;119(10):2914–2924.
46. Braconi C, et al. microRNA-29 can regulate expression of the long non-coding RNA gene MEG3 in hepatocellular cancer. *Oncogene*. 2011;30(47):4750–4756.
47. Tumaneng K, et al. YAP mediates crosstalk between the Hippo and PI(3)K–TOR pathways by suppressing PTEN via miR-29. *Nat Cell Biol*. 2012;14(12):1322–1329.
48. Yan J, et al. MiR-148a regulates MEG3 in gastric cancer by targeting DNA methyltransferase 1. *Med Oncol*. 2014;31(3):879.
49. Michalik KM, et al. Long noncoding RNA MALAT1 regulates endothelial cell function and vessel growth. *Circ Res*. 2014;114(9):1389–1397.
50. Ruan W, Zhao F, Zhao S, Zhang L, Shi L, Pang T. Knockdown of long noncoding RNA MEG3 impairs VEGF-stimulated endothelial sprouting angiogenesis via modulating VEGFR2 expression in human umbilical vein endothelial cells. *Gene*. 2018;649:32–39.
51. Kathiriya JJ, et al. Galectin-1 inhibition attenuates profibrotic signaling in hypoxia-induced pulmonary fibrosis. *Cell Death Discov*. 2017;3:17010.
52. Bodempudi V, et al. miR-210 promotes IPF fibroblast proliferation in response to hypoxia. *Am J Physiol Lung Cell Mol Physiol*. 2014;307(4):L283–L294.
53. Orzol P, Holcakova J, Nekulova M, Nenutil R, Vojtesek B, Coates PJ. The diverse oncogenic and tumour suppressor roles of p63 and p73 in cancer: a review by cancer site. *Histol Histopathol*. 2015;30(5):503–521.
54. Petitjean A, et al. Properties of the six isoforms of p63: p53-like regulation in response to genotoxic stress and cross talk with DeltaNp73. *Carcinogenesis*. 2008;29(2):273–281.
55. Murray-Zmijewski F, Lane DP, Bourdon JC. p53/p63/p73 isoforms: an orchestra of isoforms to harmonise cell differentiation and response to stress. *Cell Death Differ*. 2006;13(6):962–972.
56. Romano RA, Ortt K, Birkaya B, Smalley K, Sinha S. An active role of the DeltaN isoform of p63 in regulating basal keratin genes K5 and K14 and directing epidermal cell fate. *PLoS ONE*. 2009;4(5):e5623.
57. Koster MI, Kim S, Mills AA, DeMayo FJ, Roop DR. p63 is the molecular switch for initiation of an epithelial stratification program. *Genes Dev*. 2004;18(2):126–131.
58. Grob TJ, et al. Human delta Np73 regulates a dominant negative feedback loop for TAp73 and p53. *Cell Death Differ*. 2001;8(12):1213–1223.
59. Nisticò P, Bissell MJ, Radisky DC. Epithelial-mesenchymal transition: general principles and pathological relevance with special emphasis on the role of matrix metalloproteinases. *Cold Spring Harb Perspect Biol*. 2012;4(2):a011908.
60. Wendt MK, Balanis N, Carlin CR, Schiemann WP. STAT3 and epithelial-mesenchymal transitions in carcinomas. *JAKSTAT*. 2014;3(1):e28975.
61. Terashima M, Tange S, Ishimura A, Suzuki T. MEG3 long noncoding rna contributes to the epigenetic regulation of epithelial-mesenchymal transition in lung cancer cell lines. *J Biol Chem*. 2017;292(1):82–99.
62. Kage H, Borok Z. EMT and interstitial lung disease: a mysterious relationship. *Curr Opin Pulm Med*. 2012;18(5):517–523.
63. Chapman HA. Epithelial-mesenchymal interactions in pulmonary fibrosis. *Annu Rev Physiol*. 2011;73:413–435.
64. Willis BC, et al. Induction of epithelial-mesenchymal transition in alveolar epithelial cells by transforming growth factor-beta1: potential role in idiopathic pulmonary fibrosis. *Am J Pathol*. 2005;166(5):1321–1332.
65. Larue L, Bellacosa A. Epithelial-mesenchymal transition in development and cancer: role of phosphatidylinositol 3' kinase/AKT pathways. *Oncogene*. 2005;24(50):7443–7454.
66. Vaughan AE, Chapman HA. Regenerative activity of the lung after epithelial injury. *Biochim Biophys Acta*. 2013;1832(7):922–930.
67. Brabletz T, Kalluri R, Nieto MA, Weinberg RA. EMT in cancer. *Nat Rev Cancer*. 2018;18(2):128–134.
68. Guo M, Wang H, Potter SS, Whitsett JA, Xu Y. SINCERA: A pipeline for single-cell RNA-seq profiling analysis. *PLoS Comput Biol*. 2015;11(11):e1004575.
69. Heinz S, et al. Simple combinations of lineage-determining transcription factors prime cis-regulatory elements required for macrophage and B cell identities. *Mol Cell*. 2010;38(4):576–589.